ADVANCED MATERIALS TECHNOLOGIES
www.advmattechnol.de

Liquid Plug Motion Noninvasive Detecting in Opaque Microchannels via Grating Electrodes-Based Liquid-Solid Nanogenerator

Nannan Zhao, Hengxu Du, Meng Zou, Ziyue Xi, Hengyi Yang, Bowen Dong, Yawei Wang, Hongyong Yu, Ruijiang Xu, Fangyang Dong, Huiwen Wang, and Minyi Xu**

The precision in controlling fluid flow is crucial for the efficiency of microchannel devices. Consequently, it is essential to monitor the fluid within microchannels in real time. However, the microchannel flow's susceptibility to disturbance and small size present challenges in sensing. A Liquid-Solid Triboelectric Nanogenerator (TENG) with grating electrodes is proposed for non-invasive sensing of liquid plug movements in microchannels and is suitable for use with opaque channels. This sensor operates on the principle of initiating multiple pulse signals via grating electrodes. And analyze the motion of the liquid plug by the time difference between the signal peaks. It facilitates the measurement of liquid plug count, average speed, average acceleration, and the detection of flow direction. The liquid plug counters, and flow direction sensors yielded clear and distinguishable signals. The liquid plug average speed sensor achieves a 95% accuracy rate, and the acceleration sensor accurately distinguishes speed trends of the liquid plug with more than 85% precision. Grating electrodes are effectively employed for motion sensing. Analyzing the motion of an object by the time difference between voltage peaks offers greater stability than voltage magnitude analysis. Four portable prototypes are designed to make them applicable for fluid sensing in microchannel devices.

1. Introduction

Multiphase flow is widespread in various industrial and medical equipment applications. In microchannels, liquids often appear as liquid plugs within the form of multiphase flow. A fluid plug refers to a liquid that fills a section of a channel. This phenomenon is typically observed in microchannels, which have an inner diameter of 3 mm or less.[1] When a channel's diameter is sufficiently small, forming a liquid plug, the liquid's surface tension predominates over gravity. This characteristic enhances the stability of the liquid plug's shape, rendering it resistant to external disturbances. As a result, a series of randomly distributed liquid plugs can form in the microchannel.[2] The ability of microchannels to manipulate the vapor-liquid interface has spurred diverse applications, including microchannel heat exchangers,[3] microchannel reactors,[4,5] medical drug delivery,[6,7] and microfluidic chips.[8]

In practical applications, the accurate manipulation and precise detection of liquid plugs directly affects the efficiency of industrial production. In microchannel reactors, monitoring the real-time movement and content of reactants in each channel is crucial to ensure the mixing and reaction rates and accuracy of multiple working fluids, as well as to minimize by-product formation. When using microfluidic droplet generation chips, it is necessary to control the number and size of droplets to ensure accuracy. The size, speed, and direction of the liquid plug varies with external thermal conditions in certain microchannel phase change heat exchangers. Thermodynamic changes are consistently reflected in the movement of the liquid plugs.[9] Monitoring the behavior of liquid working fluids can help to improve the efficiency and design of heat pipes and other categories of microchannel devices.

However, the options available for sensing and measuring the movement of liquid plugs in microchannels are few and far between. Installing a sensor small enough for these tiny channels presents a formidable challenge. Some techniques use capacitive or resistive measurements to detect fluid,[10,11] which require electrodes to be placed in the channel. First, these invasive electrodes can cause irreversible changes to the flow characteristics of the fluid in the channel. In addition, the unique electrical properties of each fluid cause a number of problems for the accuracy of the sensor.[12] This method falls short when

N. Zhao, H. Du, M. Zou, B. Dong
Institute of Marine Thermal Engineering and Thermal Science
Marine Engineering College
Dalian Maritime University
Dalian 116026, China
E-mail: znn@dlmu.edu.cn

Z. Xi, H. Yang, Y. Wang, H. Yu, R. Xu, F. Dong, H. Wang, M. Xu
Dalian Key Laboratory of Marine Micro/Nano Energy and Self-powered Systems
Marine Engineering College
Dalian Maritime University
Dalian 116026, China
E-mail: xuminyi@dlmu.edu.cn

The ORCID identification number(s) for the author(s) of this article can be found under https://doi.org/10.1002/admt.202301926

DOI: 10.1002/admt.202301926

it comes to simultaneously measuring liquid plugs of varied compositions.

Visualization is another measurement technique that depends on sophisticated high-speed camera technology. Examples include high-speed filming and particle tracking or fluorescent marker filming.[13–15] This technique allows for the measurement of almost all kinematic properties of liquid plugs, with the accuracy ceiling hinging on the camera's frame rate and post-processing methods. However, this method comes with a major drawback: it's inapplicable to liquid plugs in opaque channels. Therefore, there's an urgent need in the field of microfluidics to identify a suitable sensor that can tackle the challenges associated with multiphase flow sensing technology.

Since Wang's group introduced the triboelectric nanogenerator (TENG),[16] great strides have been made in power generation technology[17,18] and sensing methods[19–21] in various fields. A wide range of innovative applications for TENG-based self-powered energy have emerged in industry,[22] smart home furnishings,[23] and within healthcare.[24] TENG has driven unprecedented developments in energy and sensing technology across various industries,[25] and is expected to drive even more remarkable developments in flexible sensors,[26] and biomimetic sensing.[27] The mechanism of TENG, which converts mechanical energy into electrical energy, opens up thrilling possibilities for object motion sensing technologies. Liquid-solid interface Triboelectric Nanogenerator (LS-TENG) has demonstrated significant potential in energy harvesting,[28–31] paving the way for innovative liquid motion sensing solutions.

Similar to many Solid-Solid interface TENG sensing techniques, the underlying principles of these methods depend on the correlation between the parameters and the amplitude of the voltage signal.[32,33] Some researchers have developed sensing strategies that track the target's movement by analyzing the frequency of electrical pulses.[34] The principle of this approach bears similarity to those used in heart rate and grating speed measurements. Recent research in TENG has delved into utilizing machine learning and local feature recognition for signal analysis. Recent research in TENG sensing has delved into utilizing machine learning and local feature recognition for signal analysis.[35,36] These sensing technologies have been innovatively applied in a variety of contexts.

Nonetheless, these sensing methods are not perfect. The accuracy of these sensing technologies is highly dependent on the stabilization of the voltage amplitude and the quality of the electrical signal. Voltage amplitude stands as one of the most direct output characteristics of TENG, with a myriad of parameters affecting its magnitude.[37–40] Some parameters are difficult to control,[41,42] a fact that also applies to LS-TENG. Therefore, for TENG sensing applications dependent on voltage signal amplitude, it is essential to perform controlled experiments to ensure the consistency of other parameters. Designing TENG sensors for real and complex application environments is a significant challenge. Implementing the LS-TENG mode in microchannels poses an even more serious problem.

There are several other methods that leverage the characteristics of electrical signals to detect liquid in pipelines. Multiple electrode array is used to measure the height of the liquid column in the pipe that is applied to the detection of the draught of a ship.[43] Electrodes arranged at specific angles are used to detect liquid columns in annular pipelines and facilitate ship tilt detection.[44] The location of leaks is identified by analyzing the electrical signal generated by bubbles in the pipe.[45] The length of droplets on a microfluidic chip can be calculated by measuring the duration of the voltage signal generated as the droplets move across the electrode.[46] Table S1 (Supporting Information) shows a comparison of these applications.

The present work proposes a novel approach to detect liquid plug flow in microchannels. The Grating Electrodes Liquid-Solid Triboelectric Nanogenerator (GLS-TENG) facilitates non-invasive monitoring of liquid plug motion in opaque microchannels by identifying of multiple electrical pulse signals. This is achieved by connecting multiple pairs of electrodes in parallel to produce electrical signals with distinctive characteristics, enabling the detection of multiple voltage pulses in a single liquid plug movement. The sensing process does not depend on voltage amplitude or local features of the signal that carry implicit information, making this method simple and reliable. With electrodes mounted on the outside of the tube, this non-invasive detection technique does not disrupt the mass flow of the fluid, making it more suitable for opaque channels or where visualization is impractical.

2. Experimental Section

A schematic diagram of the experiment system is shown in **Figure 1a**. A plunger pump served as the liquid plug driver, an electrometer functioned as the signal detector, and a high-speed video camera confirmed the measurement outcomes. The plunger pump regulated the flow rate, ensuring consistent and uniform movement of the liquid plug within the microchannel. The syringe of the plunger pump was connected to one end of the microchannel through a hose. The plunger pump propels the empty syringe, driving the liquid plug through the microchannel while leaving the other end of the microchannel open to the atmosphere.

Figure 1b shows an enlarged view of a sensor in the experimental setup. Copper electrode rings were attached to the outside of the microchannels to assemble the four liquid plug sensors. These rings were then soldered to the wires and connected as shown in Figure 1c. The wires were connected to the electrometer and there was no need to distinguish between positive and negative terminals. Before each experiment, a micro-syringe was used to inject a predetermined volume of liquid into the microchannel. Prior to each experiment, a predetermined volume of liquid was injected into the microchannel using a micro-syringe.

Reproduction of the output voltage amplitude in each experiment was difficult to guarantee because the output voltage amplitude may vary in experiments conducted at different times with the same parameters as far as possible. Consequently, each series of experiments was conducted independently within the same time frame. To minimize the error, the experiment was repeated five times for each parameter.

The Fluorinated Ethylene Propylene (FEP), Polyvinyl Chloride (PVC), and Nylon pipes used in the experiments had an outer wall diameter of 3 mm. Three sizes of tubing with inner diameters of 1, 1.5, and 2 mm were used. The fluid media used were Deionized water (DI Water), Ethanol, and a 0.9% sodium chloride aqueous solution (NS). The electrodes were made of brass rings with an

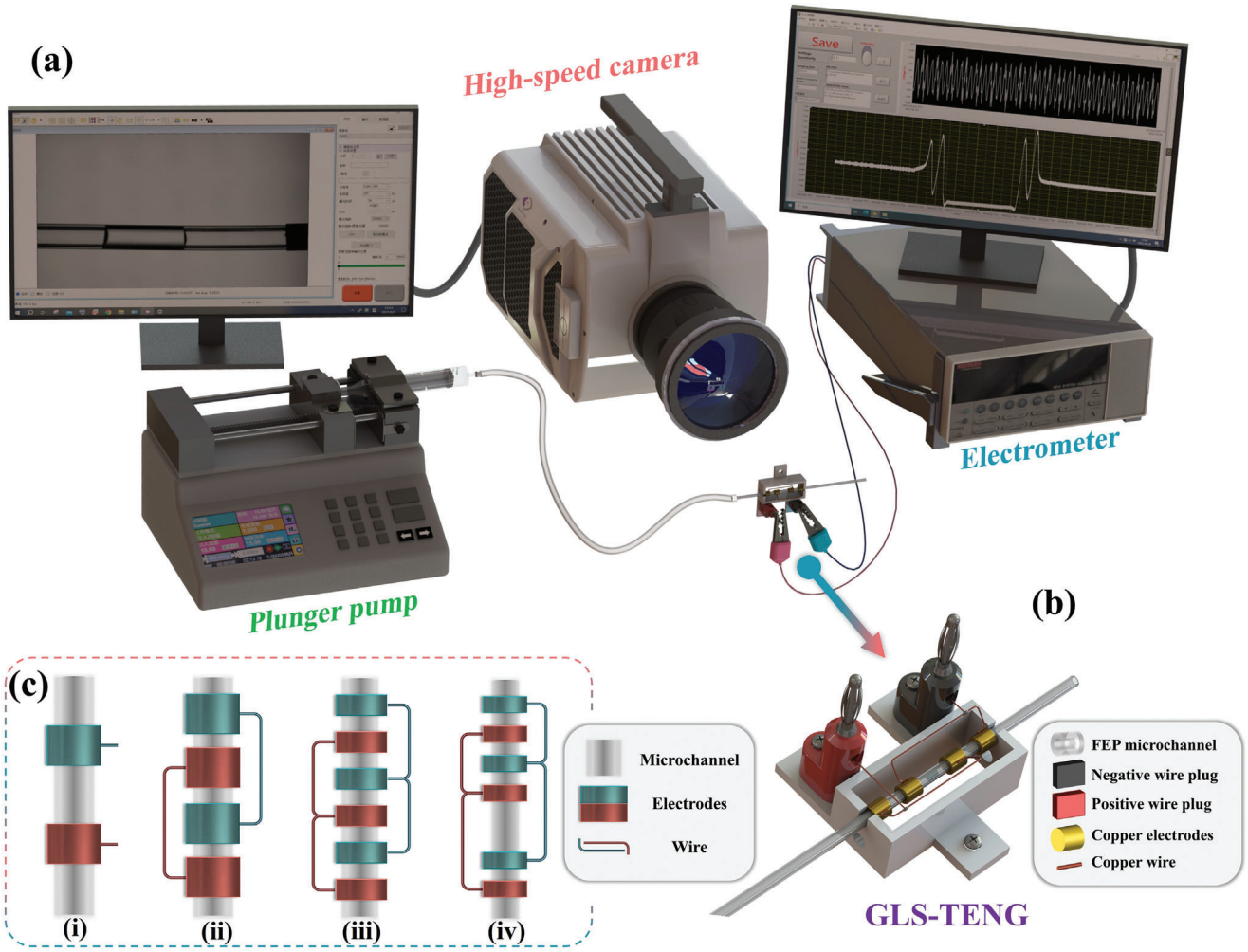

Figure 1. Schematic diagram of the experimental system. a) a partial view of a liquid plug speed sensor with two pairs of electrodes. b) Electrode connection of GLS-TENG: counter i), speed sensor ii), acceleration sensor iii), flow direction sensor iv) c).

inner wall diameter of 3 mm and an outer diameter of 5 mm. Two types of electrode rings, 3 and 5 mm in length, were used. The wires used to connect the electrodes in parallel were 0.6 mm diameter bare copper wires soldered to the outer wall of the electrode ring using soldering tin. To facilitate electrode spacing adjustment, nylon engineering plastics of various lengths, such as 3, 5, and 10 mm, with an inner diameter of 3.2 mm and an outer diameter of 7 mm, were placed between some of the electrodes. The devices were held in place by 3D-printed brackets made of PLA plastic. The bracket was equipped with internationally recognized red and black banana plugs to connect the two poles of the devices.

The voltages were measured with a Keithley 6514 electrometer. The red and black probe holders were attached to the corresponding banana plugs. A Phantom V2012 high-speed camera was used for visualization verification. The maximum resolution of the camera was 1280 × 800, with frame rates of 500 and 1000 fps. The movement of the liquid plug was facilitated by a LEAD-FLUID TYD01-01 plunger pump that pushes air into the syringe with a flow rate range of 0.184 μL mi^{-1}n to 83.318 mL min^{-1}. The syringes used were DM Disposable sterile syringes with a capacity of 20 mL. The conversion of the flow rate from the plunger pump to the flow speed in the 2 mm inner diameter microchannel is shown in Table S2 (Supporting Information). Acrylic panels and electronic components for portable products were purchased or customized from Jialichaung Company.

3. Results and Discussion

3.1. Structure and Principle of Grating Electrodes-Based LS-TENG

The fluid within the microchannel tends to form a plug flow with a random distribution of vapor bubbles and liquid plugs. The variance in dielectric constants between vapor bubbles and liquid plugs in the microchannel offers a chance to monitor liquid plug movement via TENG. The sensor is constructed of uncomplicated materials, including copper ring electrodes that combine to form a free-standing TENG electrode. These electrodes are attached to the outside of an FEP tube, which is hydrophobic and carries a negative electrical charge, thereby creating a standard tubular LS-TENG.

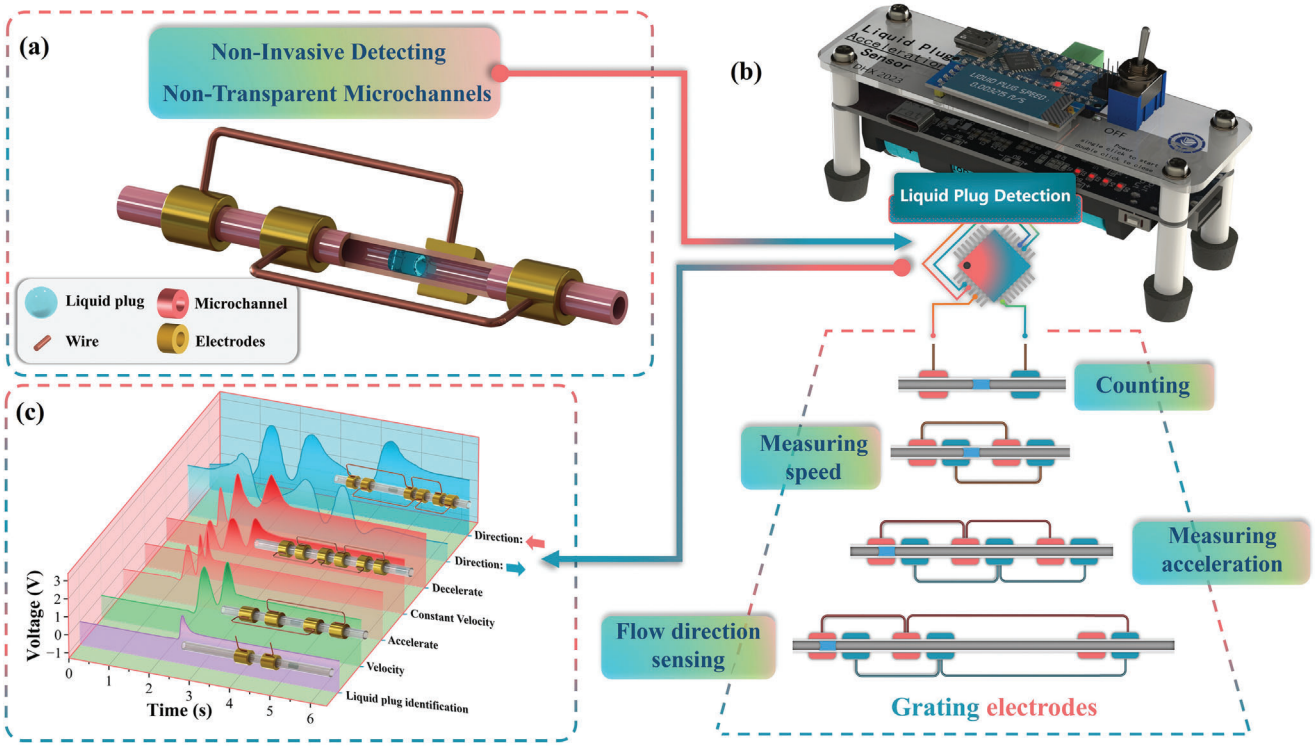

Figure 2. Structural diagram of a noninvasive grating electrode liquid-solid Triboelectric Nanogenerator suitable for detecting liquid-plug motion in opaque microchannels. a) Liquid plug sensor design blueprint. b) Comparison of voltage waveforms of four sensors under different operating conditions. c).

When a liquid plug flows through this tube-type LS-TENG, a sensitive voltage signal can be detected, enabling a liquid plug counter function. By connecting the electrodes of LS-TENGs in parallel, a GLS-TENG with a grating electrode structure is formed, which generates multiple pulse signals from the movement of a single liquid plug. **Figure** 2a shows the parallel electrode connections, where the first electrode in each LS-TENG electrode pair is connected, followed by the second electrode. Through this parallel connection, three types of sensors are developed to calculate the average speed and acceleration of the liquid plugs and to determine their flow direction. The liquid plug sensor design blueprint is shown in Figure 2b. Figure 2c shows these sensors and their voltage waveforms in operation. Based on these waveform patterns, four portable sensor products are created that are able to detect the movement of liquid plugs in real-life situations. GLS-TENG exhibits a high level of signal sensitivity, minimizing numerous unnecessary errors by forgoing signal amplitude analysis. GLS-TENG exhibits a high level of signal sensitivity, minimizing numerous unnecessary errors by forgoing signal amplitude analysis. Its non-invasive detection characteristics and suitability for opaque channels make it suitable for a wide range of microfluidic sensing applications.

3.2. Performances of Grating Electrodes-Based LS-TENG

The one-pair electrode LS-TENG consists of two copper rings mounted on FEP tubes to act as electrodes. **Figure** 3a shows the contact angle of DI Water on the flattened FEP tube wall and the surface morphology of FEP observed through a scanning electron microscope. The image at the bottom of Figure 3a, created through numerical simulation and actual photographs, displays the concave gas-liquid interface morphology of the liquid plug in the microchannel, influenced by surface tension.

Figure 3b illustrates the operating principle of the LS-TENG. Due to its free-standing structure, it can be assumed that the liquid plugs flow uniformly within the microchannels. Within the triboelectric series, water tends to exhibit positive electronegativity, in contrast to FEP, which exhibits negative electronegativity. The liquid plug surface is positively charged and the FEP tube is negatively charged by the triboelectric effect. As the liquid plug approaches the bottom of a copper electrode, it attracts electrons from the more distant copper electrode to the closer one. As a result, the more distant electrodes become positively charged and the closer electrodes become negatively charged, creating a potential difference in the external circuit. Likewise, as the liquid plug moves past the left electrode and approaches the right electrode, another electron transfer occurs in the opposite direction. The reversal of the potential results in the generation of an alternating current (AC) voltage signal.

The various parameters affecting the amplitude of the voltage signal were investigated in subsequent stages of the study. A microchannel tube was used for the experiments. By default, the outer diameter was 3 mm and the inner diameter was 2 mm. The copper electrodes used had an internal diameter of 3 mm, an external diameter of 5 mm, and a length of 5 mm, giving a

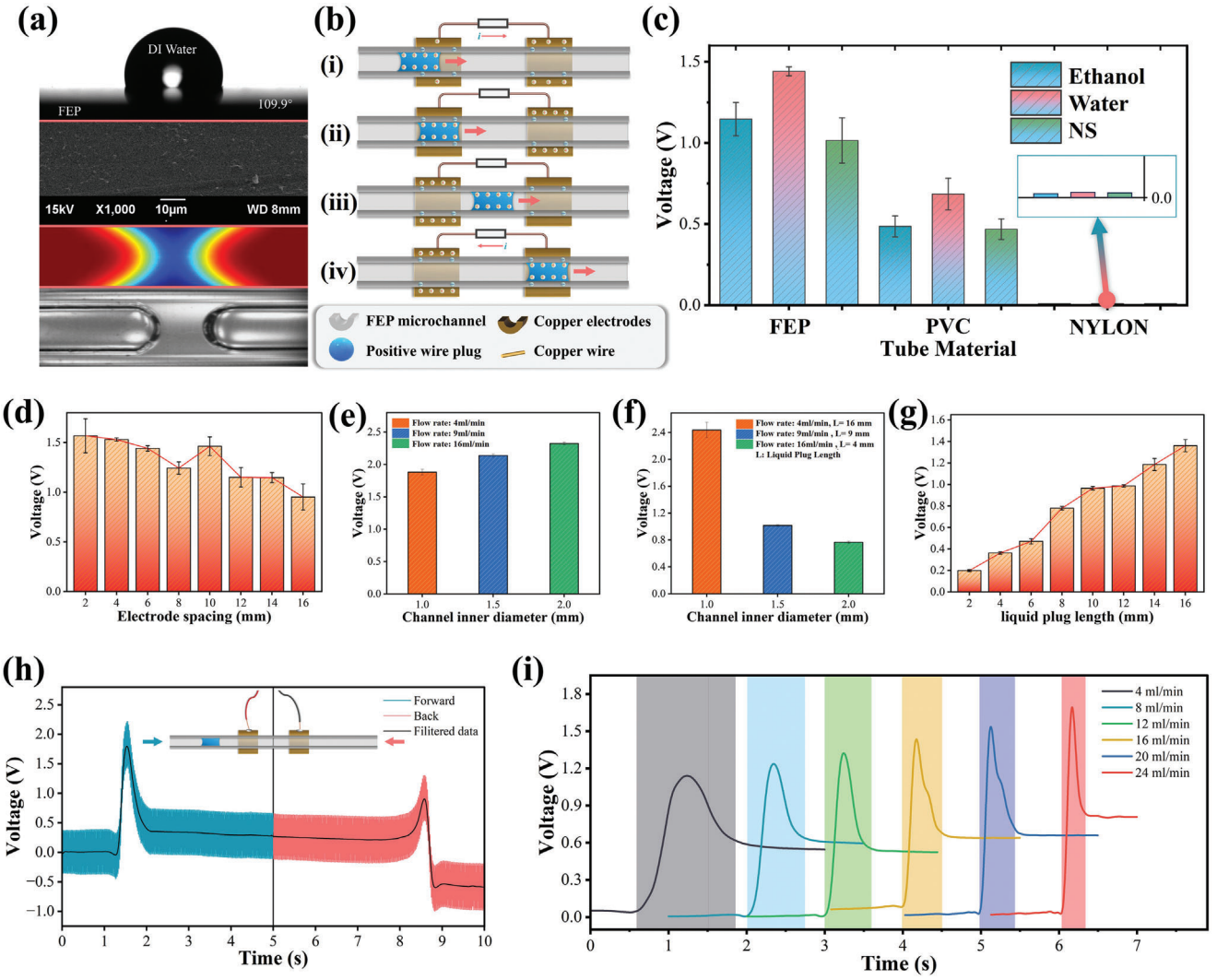

Figure 3. The contact angle of DI water on the wall of a PEP tube, the surface morphology of an FEP tube wall under scanning electron microscope and microscope, morphology simulation, and photographs of liquid plug formation in a microchannel. a) Working principle of the LS- TENG with one pair of electrodes. b) The output Voltage measured with different Liquid ingredients and tube materials c), electrode spacing d), different channel diameters but same liquid plug lengths e), different channel diameters but the same liquid volume f), and different plug lengths g) Waveform of the voltage signal detected when the liquid plug moves in different directions. h) Output voltage measured at different speeds of liquid plug movement. i).

distance of 10 mm between the edges of the two electrodes. The first factor evaluated was the material. The tubing materials used in the experiments included FEP, PVC and nylon. The liquid media used were DI Water, Ethanol, and NS. To ensure consistency, parameters such as the volume and speed of the liquid plug were carefully controlled. The results of the orthogonal experiments show that the choice of different tubes and fluids results in different voltage signal amplitudes produced by the LS-TENG, as shown in Figure 3c. This variation correlates with each material's unique ability to confine electrons. The output voltage of the LS-TENG will be close to zero in the special case where nylon is used as the channel material. This is attributed to the similarity in electron affinity between nylon and the liquids used, which are close in the sequence of triboelectric materials. This suggests that LS-TENG sensors require two materials with very different electron confinement capabilities to ensure sensor validity.

Figure 3d shows the effect of the electrode spacing on the output voltage, but does not reveal the significant pattern. Then experimented with the pipe diameter parameter. The inner diameter was set to 1, 1.5, and 2 mm and all other dimensions of the FEP microchannel were left as default. DI water was used as the liquid plug medium. In the first group, the liquid plugs had a uniform length across channels of different diameters (Figure 3e), whereas in the second group, the liquid plugs had a uniform volume (Figure 3f). Appropriate pump flow rates were determined for each channel diameter throughout the experiments to negate the effect of speed (Table S3, Supporting Information). This ensured that the liquid plugs moved at a uniform speed in each channel. Additionally, liquid plugs of different lengths were tested in a 2 mm diameter channel (Figure 3g). In the first group, the larger the diameter of the channel, the larger the contact area of the channel with the liquid plug and the higher the

voltage, while keeping the length of the liquid plug the same. In the second group, since the volume of liquid is the same, the liquid plug is the shortest in the channel with the larger diameter, and increasing the diameter of the channel causes the voltage to decrease. These experiments effectively reflect the contact area between the liquid plug and the channel wall, demonstrating that an increased contact area boosts the output voltage of the LS-TENG.

The electrical signal waveforms shown in Figure 3h were then obtained by deliberately changing the direction of movement of the fluid plug. The waveforms for both forward and backward motion show unique AC patterns but overall appear to resemble a positive pulse signal. In all of the above experiments, the slight fluctuation in voltage amplitude was partly attributed to the residual liquid remaining in the channel after the first liquid plug had passed.

Figure 3i shows the relationship between the voltage signal and liquid plug speed as the liquid plug speed is varied by the plunger pump with all other dimensions held constant. As the speed of the liquid plug increases, the amplitude of the voltage signal noticeably increases and its duration decreases, as we would intuitively expect. The faster the liquid plug moves, the higher the amplitude and the shorter the pulse duration of the voltage signal will be.

The results from these experiments are suitable for sensor development, including those aimed at composition detection, flow direction detection, liquid plug length measurement, and speed measurement. However, these parameters are just a small portion of the numerous factors that influence the output voltage, and they are relatively simple to implement. However, these are not the only parameters that can have a significant effect on the voltage amplitude of the LS-TENG. Factors that are more difficult to control, such as the ambient temperature and humidity, also play an important role. In real-world applications, these issues are unavoidable, so all parameters must be collectively considered. Therefore, a change in the amplitude of the voltage alone cannot be a definitive indication of which specific parameters have changed. However, in a carefully controlled experiment, variations in voltage amplitude can still be a powerful tool for elucidating many specific scenarios within complex questions.

In attempts to design TENG sensors, the variability of the output voltage signal, which is influenced by numerous factors, poses problems for sensor reliability. Nonetheless, it also offers fresh insights and directions for the development of sensors equipped with grating electrodes. The aforementioned experiments showed that the passage of a liquid plug through an LS-TENG equipped with a single pair of electrodes results in the generation of a single pulse signal. By positioning a certain number of LS-TENG units along the outer wall of an FEP microchannel tube, they can sequentially generate an identical number of electrical pulse signals. Following this concept, a Grating Electrode Liquid-Solid Triboelectric Nanogenerator (GLS-TENG) was developed by connecting two sets of LS-TENGs in parallel and arranging them in an intertwined pattern, as shown in **Figure** 4a.

To validate this concept, numerical simulations were performed using COMSOL Multiphysics software, using the same geometric parameters and boundary conditions to closely replicate real-world scenarios. The voltage waveform simulation approach proposed by Xie[47] was followed, and the simulated waveforms (Figure 4b) confirmed the validity of this assumption, with consistent amplitudes of the two waveforms.

As shown in Figure 4c, the principle of charge transfer on the electrodes in the GLS-TENG is also investigated. For ease of understanding, the electrodes are referred to as e1, E1, e2, and E2 (from left to right), and the corresponding charge transfers as Qe1, QE1, Qe2, and QE2. Similar to the **LS-TENG** in other research, the electrode charge transfer is driven by the electrostatic interaction between the liquid plug and the electrodes. The distinction is that the electrons at each electrode interact with a positively charged liquid plug, necessitating the loss of some electrons at each electrode to neutralize the electrostatic induction force. However, the strength of the electrostatic induction varies with the distance between the liquid plug and each electrode (Equations (1)). F is the interaction force between the charges, k is the Coulomb constant, Q_1 and Q_2 are the charges, and r is the distance between the charges. Electrostatic induction decreases with distance. Consequently, the quantity of electron transfer on each electrode varies. More electrons are required to achieve equilibrium when there is greater electrostatic induction between the electrodes and the liquid plug. In this schematic, the length of the arrows is used to indicate the amount of electron transfer or the magnitude of the potential difference (u).

$$F = k \times \frac{Q_1 \times Q_2}{r^2} \tag{1}$$

In the first stage (Figure 4c–i), as the liquid plug passes underneath e1, the positive charge on the surface of the liquid plug simultaneously attracts varying amounts of electrons from the three electrodes: E1, e2, and E2 respectively, and transfers them to e1. Since the electrostatic induction force on E2 is the weakest, it requires only a small number of electrons to reach equilibrium. So E2 transfers the most electrons, while E1 transfers the fewest. However, some electrons are transferred directly from e2 to e1 because e2 is bonded to e1. The overall effect of the amount of charge transferred to the external path by this route is shown in Equation (2), at which point the voltage waveform shows an upward trend.

$$|Q_{e1}| = |Q_{E1}| + |Q_{E2}| \tag{2}$$

In the second stage (Figure 4c–ii), the liquid plug moves to the center of e1 and E1, where they are in similar states, causing the charge transfer between them to cancel out. At this stage, some electrons from e2 and E2 are taken by e1 and E1, respectively. Since the electrostatic induction on E2 is comparatively weaker than on e2, it requires fewer electrons than e2. As a result, E2 assumes a more pivotal role in utilizing electrons to offset the positive charge between E1 and e1. Overall, a limited number of electrons are still transferred from E2 to e1 via the external path. Although the charge transfer at this point is minimal, it aligns directionally with the first stage. The potential difference is at its maximum at this position, corresponding to the moment when the first peak appears in the waveform.

In the third stage (Figure 4c–iii), the liquid plug reaches a position just underneath E1. The charge transfer of this stage mirrors that of the first stage, but in the opposite direction. The overall effect of charge transfer via the external path at this stage is

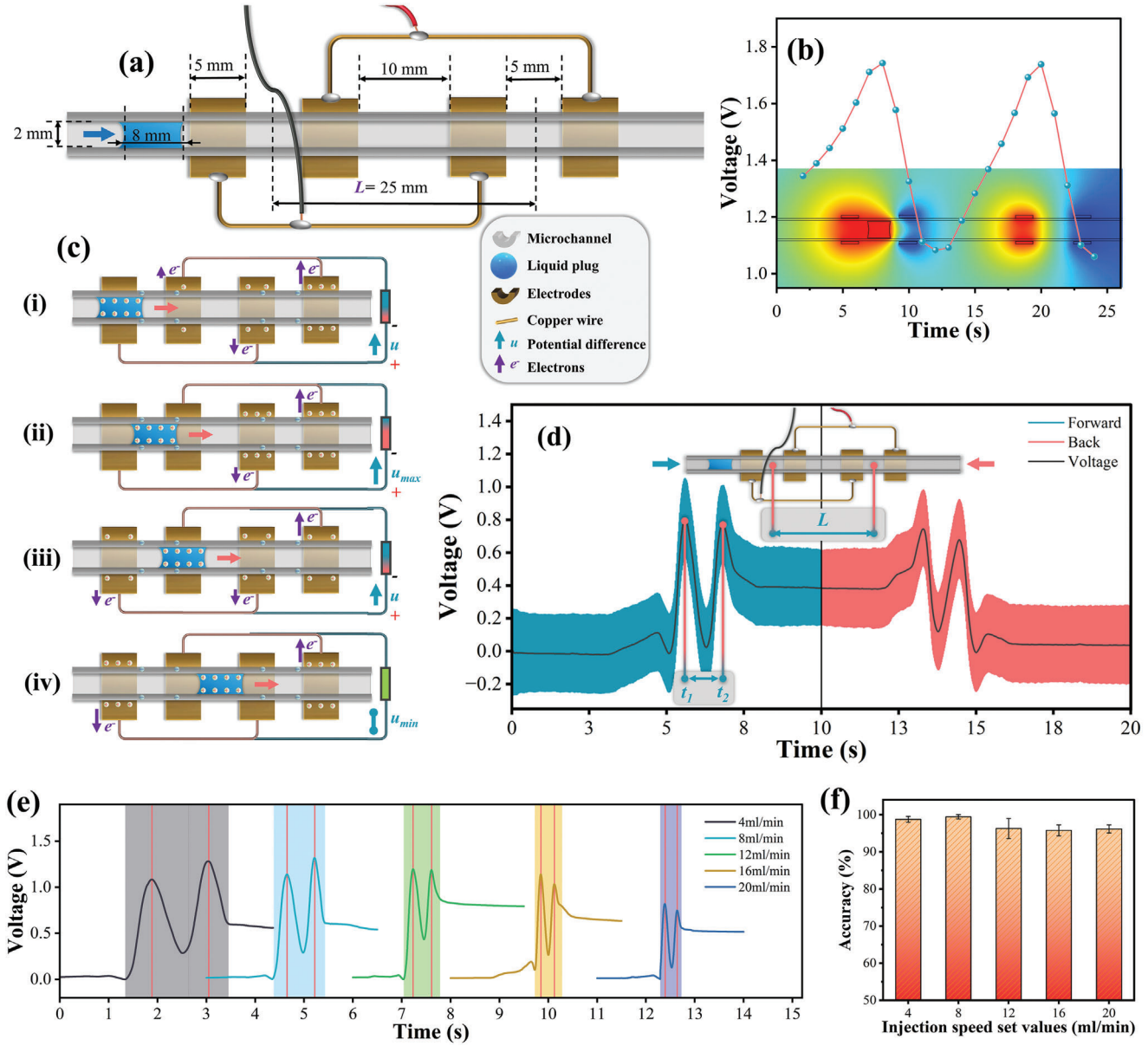

Figure 4. Liquid Plug Speed Sensor Dimensions. a) Waveforms of a liquid plug speed sensor simulated numerically in COMSOL. b) Working principle of the liquid plug speed sensor. c) Waveform of the voltage signal detected when the liquid plug moves in the speed sensor. d) Waveforms of voltage signals are detected in the liquid plug speed sensor when the liquid plug moves at different speeds. e) Accuracy of the measurement results of the liquid-plug speed sensor in comparison with the visualized measurement results. f).

outlined in Equation (3). As the direction of charge transfer along the external path is reversed, the potential difference between the two pairs of electrodes gradually disappears, resulting in a falling voltage waveform.

$$|Q_{E1}| = |Q_{e1}| + |Q_{e2}| \tag{3}$$

In the fourth stage (Figure 4c–iv), the liquid plug enters the gap between E1 and e2, with the electrostatic induction effects on each pair of electrodes being symmetrical. By bypassing the external circuit, electron transfer takes place exclusively between the connected electrodes. Consequently, external charge transfer is minimized in this stage, signifying the end of the first voltage waveform pulse, which drops to its lowest level. In the next stage, the liquid plug moves to the right half of the GLS-TENG and follows the same charge transfer process as the previous four stages. So, the complete voltage waveform has two pulses. It is particularly important to emphasize that the position of the peaks corresponds to the center of each pair of electrodes.

The moment at which the liquid plug reaches the center of e1 and e2 is called t_1 and the moment at which the center of E1 and E2 are reached is called t_2. The distance between the centers of the two pairs of electrodes is set at 25 mm. Thus, the average speed of the liquid plug can be easily calculated by dividing the

displacement (L) by the time interval ($t_2 - t_1$). Figure 4d shows the voltage signal waveform generated as the liquid plug traverses the GLS-TENG, marked by two pairs of electrodes, peak moments (t_1 and t_2), and displacement (L). The average speed v_{mean} is calculated using Equation (4).

$$v_{mean} = \frac{L}{t_2 - t_1} \tag{4}$$

This principle makes it possible to use a GLS-TENG with two pairs of electrodes as a sensor for measuring the speed of liquid plugs. In this experiment, the plunger pump pushed the air inside the syringe, propelling the liquid plug inside the microchannel and ensuring uniform movement. There are limits to the precision of the injection pump. The visual speed measurement data is used for comparison to ensure that the liquid plug speed is its actual moving speed. A high-speed camera was used to capture real-time images of the microchannels as the liquid plugs moved through them. Transparent microchannels were therefore used for the experiments. After each experiment, the actual speed of the liquid plug was assessed using visual velocimetry and compared with the speed calculated from the voltage waveform.

Figure 4e shows the voltage signal waveforms produced by the same liquid plug at five different speeds. Increasing the speed results in a shorter pulse duration, as with the LS-TENG. For an electrical signal with two peaks, a higher speed results in a shorter time interval between the peaks, in line with intuitive expectations. The speeds calculated from the waveforms were then compared with actual measurements, showing that this method of speed measurement is more than 95% accurate (Figure 4f). This is a simple and very accurate way of measuring the speed, which is a satisfactory result.

Inspired by the average speed measurements in the previous section, acceleration measurements can be realized by simply adding a pair of equally spaced electrodes to the liquid plug speed sensor. The principle of electron transfer is the same as the speed sensor. Subsequently, three pairs of electrodes are arranged in parallel, with the method of parallel connection and detailed dimensional parameters shown in **Figure** 5a. There should be three peaks after passing through a liquid plug.

The feasibility of the acceleration measurement conjecture was verified in COMSOL Multiphysics by configuring three pairs of equidistant electrodes. In conventional TENG simulations, only the steady state waveform of the uniform linear motion of the liquid plug can be simulated using the Parameter Sweep method. To simulate the variable speed movement of the liquid plug, it is necessary to define an additional function nested within the parameter to be swiped. An interpolating motion coordinate-time function is illustrated here with an initial speed of 0 mm $^{-1}$s and an acceleration of + 0.1 mm $^{-1}$s^2. The liquid plug will follow this function during the parameter sweep, and the specific coordinate settings are presented in Table S4 (Supporting Information). The speed change of the liquid plug movement and the coordinate change graph are shown in Figure S7 (Supporting Information), and the three peak times are marked (Figure S7b, Supporting Information). In the simulated waveform result (Figure 5c), three pulse signals emerge and the time gap between the peaks becomes progressively smaller.

The results of the actual experiment are also in line with the conjecture, as follows. The time interval between the three peaks gradually decreases as the liquid plug accelerates. During uniform motion, the time interval between the peaks remains constant. Conversely, during deceleration, the time interval between the three peaks gradually increases, as shown in the actual waveform in Figure 5b.

Figure 5d shows the waveform generated by a liquid plug moving back and forth at a uniform speed within the channel of the acceleration sensor. The time instants of the three wave peaks are denoted as t_1, t_2, and t_3, and the displacement of the liquid plug is 2×l. All these parameters can be measured. The average acceleration, expressed as a_{mean}, is calculated using Equation (5).

$$a_{mean} = \frac{v_2 - v_1}{\Delta t} = \frac{\frac{l}{t_3 - t_2} - \frac{l}{t_2 - t_1}}{t_3 - t_1} \tag{5}$$

After verifying the calculated results with a high-speed camera, it was found that the accuracy of the liquid plug acceleration sensor exceeded 85% (Figure 5e). GLS-TENG accurately identifies trends in speed changes of liquid plugs within microchannels. This method is an aid to identifying fluid flow behavior.

Furthermore, by modifying the spacing between the electrodes, the GLS-TENG equipped with three pairs of electrodes was converted into a sensor for detecting the direction of liquid plug flow. Specifically, two pairs of electrodes were placed closer together, while the third pair was placed further apart, as shown in Figure 5f. Given the uneven spacing between these three pairs of electrodes and the wave peaks that occur in the center of each pair of electrodes, the time intervals between the three pulse signals should be uneven when a liquid plug is flowing uniformly. This type of waveform was also simulated in COMSOL Multiphysics (Figure 5g).

As shown in Figure 5h, as the liquid plug moves from left to right at a uniform speed, it first encounters two closely spaced pairs of electrodes, resulting in two adjacent pulse signals. Subsequently, as the liquid plug moves through the region without electrodes, the waveform exhibits no significant undulation. Finally, the third waveform begins to appear as the fluid plug reaches the last pair of electrodes. Conversely, a symmetrical waveform will be generated if the liquid plug flows uniformly from right to left within the microchannel. Physical and rendered views of the GLS-TENGs (liquid plug averaged acceleration sensor and flow direction sensor) with three pairs of electrodes are shown in Figure 5i,j. This provides an innovative method for detecting the direction of motion of a liquid plug in an opaque channel.

3.3. Demonstration of Grating Electrodes based LS-TENG

Figure 6a(i–iv) shows the electrode connections of the four sensors, sample waveforms, and signal peak sampling method. Video S1–S4 (Supporting Information) further demonstrates their features. These sensors are based on analyzing the frequency characteristics of pulse occurrences and do not consider the voltage signal amplitude, which improves accuracy by limiting uncontrollable conditions.

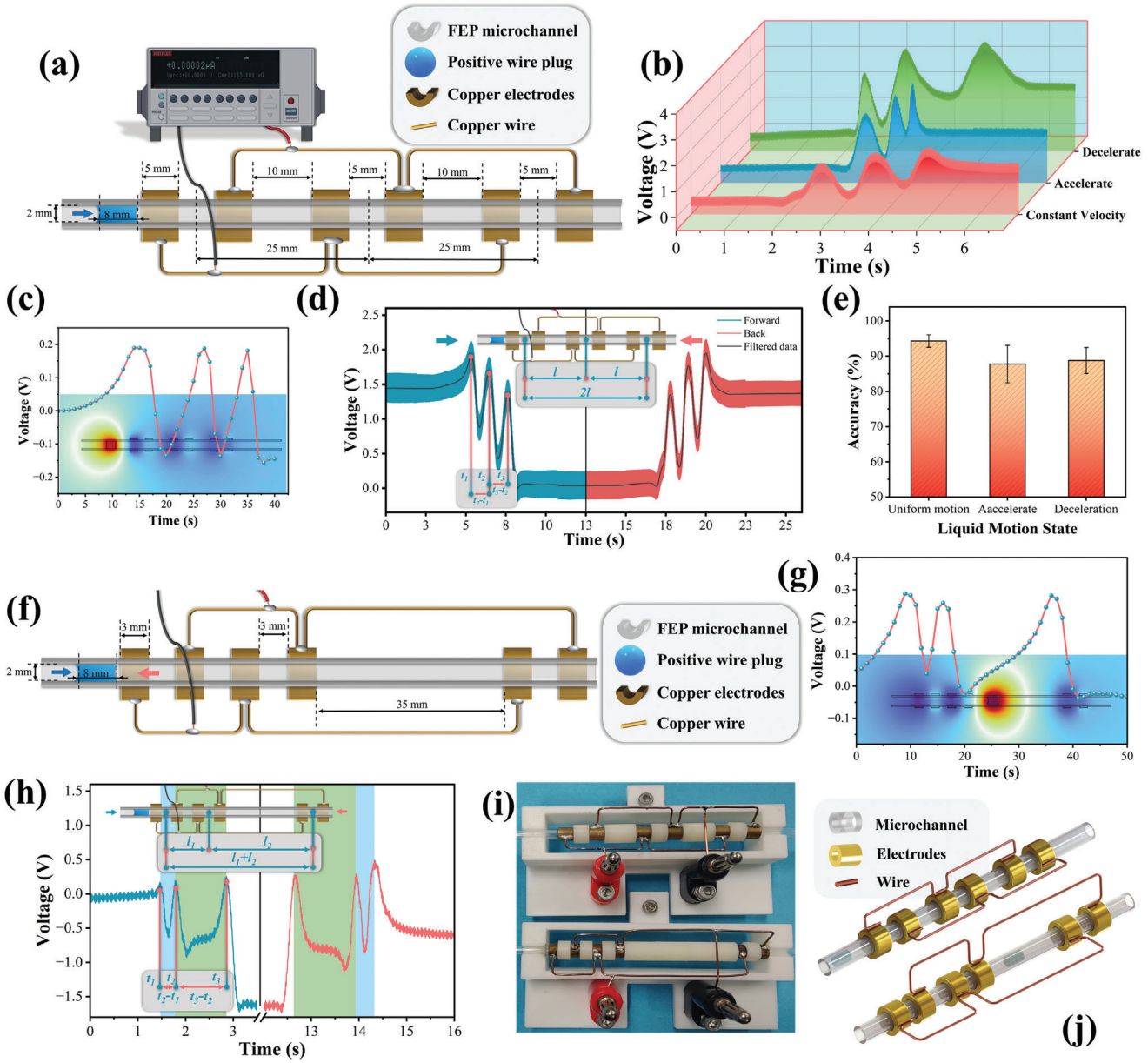

Figure 5. Dimensional parameters of liquid plug acceleration sensors. a) Voltage signal waveforms of the liquid plug in the liquid plug acceleration sensor at constant speed, acceleration, and deceleration, respectively. b) Voltage waveform of a liquid plug accelerating through a liquid plug acceleration sensor simulated with COMSOL. c) Examples of voltage waveforms when the liquid plug moves uniformly in a liquid plug acceleration sensor and sampling points for acceleration calculation. d) Accuracy of the measurement results of the liquid-plug acceleration sensor in comparison with the visualized measurement results. e) Dimensional parameters of liquid plug flow direction sensors. f) The voltage waveform of a liquid plug accelerating through a liquid plug flow direction sensor was simulated with COMSOL. g) Voltage waveforms of the liquid plug moving in different directions in the liquid plug flow direction sensor and sampling points for determining the flow direction. h) Photographs (i) and schematics (j) of liquid plug acceleration sensors and liquid plug flow direction sensors.

To implement these sensing methods, four portable sensors were constructed to count liquid plugs, measure average liquid plug speed, calculate average liquid plug acceleration, and sense liquid plug flow direction. An 18 650 Li-ion battery powers the entire sensing system, and an Arduino Nano serves as the controller, as shown in Figure 6c. The devices are connected to the sensor via an Analog pin (A0) and a Ground pin (GND) as the sensing pins. The Arduino Nano incorporates a filtering algorithm that stabilizes the signal and boosts anti-interference performance (Video S5, Supporting Information). Then processes filtered signals, calculates results, and displays them on the OLED screen. Figure S5 (Supporting Information) shows the structural design of four portable sensors. Figure 6d provides a rendered model of the overall structure of a liquid plug sensor (acceleration sensor), and Video S6 (Supporting Information) demonstrates

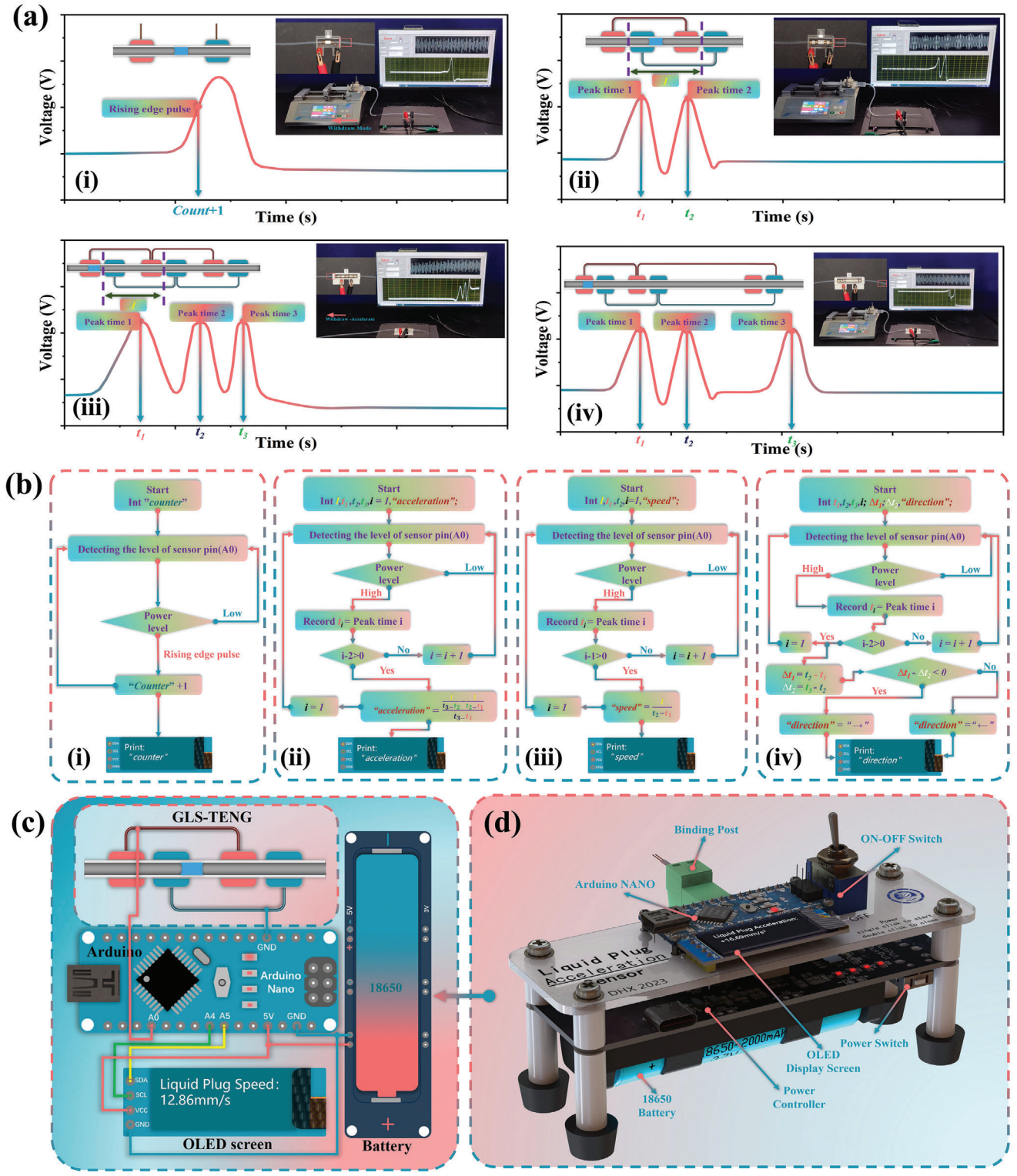

Figure 6. Voltage waveforms and sampling point diagrams of four types of liquid-plug motion sensors. a) Block diagram of the operation program of the portable sensor for liquid plug counter; b) liquid plug average speed sensor; c) liquid plug average acceleration d) and liquid plug flow direction sensor. e) System diagram for the circuit design of the portable sensor. f) Rendering of the structure of a portable sensor for detecting the movement of a liquid plug. g).

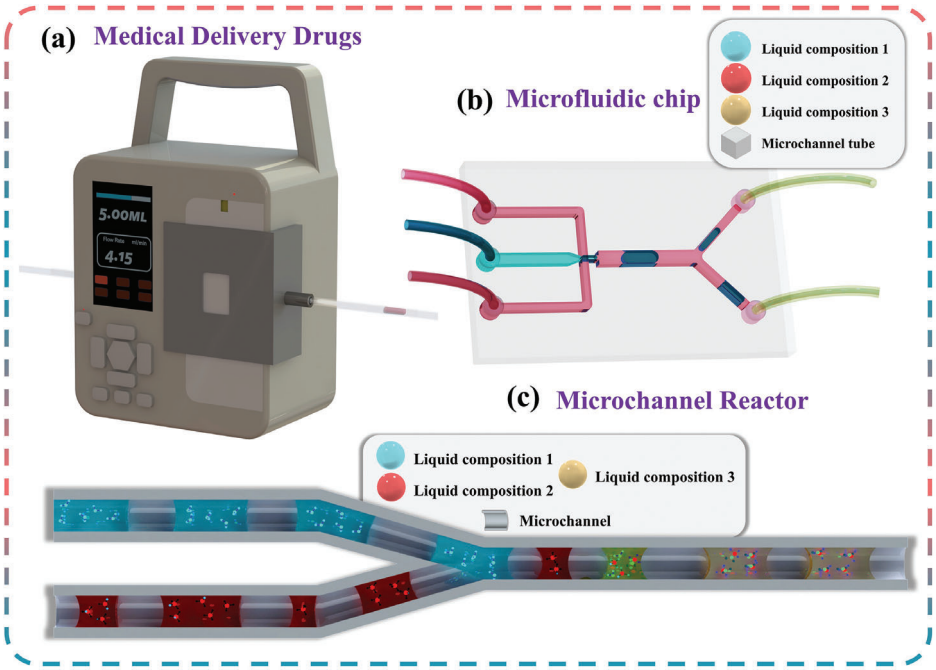

Figure 7. Medical drug delivery. a) Microfluidic chip. b) Microchannel reactors. c).

the functionality of these four microchannel liquid plug sensors.

Figure 6b(i–iv) shows the block diagram of the design program for these four sensors. Connect the pin of the sensor according to the corresponding color before use. The liquid plug counter senses the voltage value of the LS-TENG via the "A0" Analog measurement pin, and records and filters the data. The "*Counter*" is incremented by "*1*" when the voltage exceeds the predefined threshold. When the voltage is detected above the set threshold, add "*1*" to the "*Counter*". Then, proceed with a "Delay" before the next count cycle. In the same way, the speed sensor of the liquid plug records the data of the voltage values and the peak times (*peak time 1, 2*) above the threshold from the "A0" pin. Once the two peaks have been recorded, it calculates the difference in time ($t2 - t1$). Then, it computes the average speed of the liquid plug movement based on the electrode spacing (l). The liquid plug acceleration sensor will record continuous peaks three times (*Peak time 1,2,3*). Take in the set electrode spacing (l) and solve the average acceleration of the liquid plug according to Equation (5). Similarly, three consecutive peak times are recorded by the liquid plug movement direction sensor. The time difference ($\Delta t1$, $\Delta t2$) between each two adjacent peak moments is then calculated. The direction of liquid plug movement is determined by comparing the values of "$\Delta t1$" and "$\Delta t2$".

GLS-TENG is applicable to a range of microchannel devices. For high-precision medical drug delivery systems (**Figure** 7a), the installation of liquid plug counters and speed sensors enables more accurate dosage control. It can also detect harmful air bubbles in medical infusion lines. In biological or chemical microfluidic chips (Figure 7b), this method can replace traditional visualization methods for droplet counting and droplet generation rate detection. In microchannel reactors, sensors can also be attached to the microchannels to monitor chemical fluid transport. Figure 7c shows a simple example where two chemical liquids, blue and red, mix and react to form chemical liquid component 3. Liquid plug counters and velocity sensors can be mounted on the pipe wall to track the dosing, delivery and reaction rates of the different reactants. The GLS-TENG is a significant breakthrough in the field of liquid plug flow sensing and its development may lead to further advances in microfluidic technologies.

4. Conclusion

In this work, the pattern of the electrical pulse signal was found by testing the effect of various parameters on the LS-TENG voltage signal. This pattern was then used to develop the GLS-TENG, which is capable of accurately detecting the motion characteristics of liquid plugs in microchannels. The sensors achieve an accuracy rate of 95% in the calculation of the average speed of the liquid plug and an accuracy rate of more than 85% in the calculation of the average acceleration. Additionally, they precisely count liquid plugs and accurately identify the flow direction. Based on these designs, four prototypes were fabricated, which have significantly increased the practical value of the GLS-TENG sensors. These non-invasive electrodes have minimal impact on fluid flow characteristics in microchannels and are more cost effective than visual observation methods. They are also suitable for use in opaque channels or confined environments where visual inspection is impractical. Unlike methods that analyze parameter changes by voltage amplitude, the GLS-TENG method offers higher accuracy, making it ideal for high-precision microfluidic sensing. This new method of monitoring fluids within microchannel devices could guide improvements to these devices to significantly increase efficiency.

Furthermore, this technique opens up new opportunities for structural innovation in TENG sensors. Grating electrodes are

particularly suitable for detecting target motion behavior. Using grating electrodes, multiple signals can be detected in a single movement of a single target. Unlike previous detection modes that depend solely on voltage amplitude, grating electrodes only rely on the presence of voltage pulse signals, which can eliminate most unstable factors. This makes it well suited for applications such as rotational speed measurement, movement monitoring, displacement detection, trajectory detection, motion trend detection, motion posture, etc.

Supporting Information

Supporting Information is available from the Wiley Online Library or from the author.

Acknowledgements

This research work was supported by the Fundamental Research Funds for the Central Universities of China under Grant No. 3132023528.

Conflict of Interest

The authors declare no conflict of interest.

Data Availability Statement

The data that support the findings of this study are available from the corresponding author upon reasonable request.

Keywords

grating electrodes, liquid plug, microchannel, triboelectric nanogenerator

Received: November 11, 2023
Revised: February 28, 2024
Published online:

[1] S. G. Kandlikar, W. J. Grande, *Heat Transf. Eng.* **2003**, *24*, 3.
[2] Z. Wu, B. Sundén, *Renew. Sustain. Energy Rev.* **2014**, *40*, 11.
[3] H. Akachi, *US4921041A*, **1990**.
[4] J. R. Burns, C. Ramshaw, *Chem. Eng. Res. Des.* **1999**, *77*, 206.
[5] V. Hessel, P. Löb, H. Löwe, G. Kolb, *Micro Instrumentation: for High Throughput Experimentation and Process Intensification - A Tool for PAT*, Wiley, Germany **2007**.
[6] K. S. Lim, M. Baptista, S. Moon, T. B. F. Woodfield, J. Rnjak-Kovacina, *Trends Biotechnol.* **2019**, *37*, 1189.
[7] R. Natu, S. Guha, S. A. R. Dibaji, L. Herbertson, *Micromachines* **2020**, *11*, 886.
[8] L. Shang, Y. Cheng, Y. Zhao, *Chem. Rev.* **2017**, *117*, 7964.
[9] H. Ma, *Oscillating Heat Pipes*, Springer, New York **2015**.
[10] A. K. Jana, G. Das, P. K. Das, *Chem. Eng. Sci.* **2006**, *61*, 1500.
[11] E. dos Reis, J. Goldstein Leonardo, *Flow Meas. Instrum.* **2010**, *21*, 347.
[12] Q. Y. Yang, N. D. Jin, L. S. Zhai, D. Y. Wang, F. Wang, *Exp. Therm. Fluid Sci.* **2019**, *107*, 16.
[13] R. Zeighami, D. Laser, P. Zhou, M. Asheghi, S. Devasenathipathy, T. Kenny, J. Santiago, K. Goodson, *Thermomechanical Phenom. Electron. Syst. -Proceedings Intersoc. Conf.* Las Vegas, NV, May **2000**, *2*, 148.
[14] M. R. Bown, J. M. MacInnes, R. W. K. Allen, *Exp. Fluids* **2007**, *42*, 197.
[15] S. J. Lee, S. Kim, *Microfluid. Nanofluidics* **2009**, *6*, 577.
[16] F. R. Fan, Z. Q. Tian, Z. L. Wang, *Nano Energy* **2012**, *1*, 328.
[17] H. Yu, Z. Xi, Y. Zhang, R. Xu, C. Zhao, Y. Wang, X. Guo, Y. Huang, J. Mi, Y. Lin, T. Du, M. Xu, *Nano Energy* **2023**, *107*, 108182.
[18] Y. Wang, Z. Qian, C. Zhao, Y. Wang, K. Jiang, J. Wang, Z. Meng, F. Li, C. Zhu, P. Chen, H. Wang, M. Xu, *Adv. Mater. Technol.* **2023**, *8*, 1.
[19] C. Zhao, Z. Wang, Y. Wang, Z. Qian, Z. Tan, Q. Chen, X. Pan, M. Xu, Y. C. Lai, *Adv. Funct. Mater.* **2023**, *33*, 2306381.
[20] T. Du, F. Dong, R. Xu, Y. Zou, H. Wang, X. Jiang, Z. Xi, H. Yuan, Y. Zhang, P. Sun, M. Xu, *Adv. Mater. Technol.* **2022**, *7*, 1.
[21] Y. Wang, D. Liu, Z. Hu, T. Chen, Z. Zhang, H. Wang, T. Du, S. L. Zhang, Z. Zhao, T. Zhou, M. Xu, *Adv. Mater. Technol.* **2021**, *6*, 2001270.
[22] M. Lian, J. Sun, D. Jiang, M. Xu, Z. Wu, B. Bin Xu, H. Algadi, M. Huang, Z. Guo, *Nanotechnology* **2023**, *34*, 025401.
[23] M. Lian, J. Sun, D. Jiang, Q. Sun, Z. M. El-Bahy, H. M. Abo-Dief, M. A. Salem, H. M. Ali, Q. Xu, Z. Guo, *J. Mater. Chem. A* **2022**, *10*, 24353.
[24] Z. Liu, Y. Hu, X. Qu, Y. Liu, S. Cheng, Z. Zhang, Y. Shan, R. Luo, S. Weng, H. Li, H. Niu, M. Gu, Y. Yao, B. Shi, N. Wang, W. Hua, Z. Li, Z. L. Wang, *Nat. Commun.* **2024**, *15*, 1.
[25] D. Jiang, M. Lian, M. Xu, Q. Sun, B. Bin Xu, H. K. Thabet, S. M. El-Bahy, M. M. Ibrahim, M. Huang, Z. Guo, *Adv. Compos. Hybrid Mater.* **2023**, *6*, 1.
[26] N. Wen, L. Zhang, D. Jiang, Z. Wu, B. Li, C. Sun, Z. Guo, *J. Mater. Chem. A* **2020**, *8*, 25499.
[27] J. Liu, P. Xu, B. Liu, Z. Xi, Y. Li, L. Guo, T. Guan, P. Zhu, Z. Meng, S. Wang, H. Wang, M. Xu, *Small* **2023**, *2308491*, 1.
[28] Z. H. Lin, G. Cheng, S. Lee, K. C. Pradel, Z. L. Wang, *Adv. Mater.* **2014**, *26*, 4690.
[29] Z. H. Lin, G. Cheng, L. Lin, S. Lee, Z. L. Wang, *Angew. Chemie – Int. Ed.* **2013**, *52*, 12545.
[30] G. Zhu, Y. Su, P. Bai, J. Chen, Q. Jing, W. Yang, Z. L. Wang, *ACS Nano* **2014**, *8*, 6031.
[31] R. I. Haque, A. Arafat, D. Briand, *J. Phys. Conf. Ser.* **2019**, 012084, https://doi.org/10.1088/1742-6596/1407/1/012084.
[32] B. D. Chen, W. Tang, C. He, T. Jiang, L. Xu, L. P. Zhu, G. Q. Gu, J. Chen, J. J. Shao, J. J. Luo, Z. L. Wang, *Adv. Mater. Technol.* **2018**, *3*, 1.
[33] J. Wang, Z. Wu, L. Pan, R. Gao, B. Zhang, L. Yang, H. Guo, R. Liao, Z. L. Wang, *ACS Nano* **2019**, *13*, 2587.
[34] Y. Liu, D. Li, Y. Hou, Z. L. Wang, *Adv. Mater. Technol.* **2023**, *8*, 1.
[35] X. Zhang, Y. Zheng, D. Wang, F. Zhou, *Nano Energy* **2017**, *40*, 95.
[36] L. Liang, X. Wang, M. Li, Z. Wang, M. Jiang, Y. Wu, H. Zheng, *Nano Energy* **2023**, *117*, 108935.
[37] R. D. I. G. Dharmasena, J. H. B. Deane, S. R. P. Silva, *Adv. Energy Mater.* **2018**, *8*, https://doi.org/10.1002/aenm.201802190.
[38] R. D. I. G. Dharmasena, S. R. P. Silva, *Nano Energy* **2019**, *62*, 530.
[39] Y. Yu, Q. Gao, D. Zhao, X. Li, Z. L. Wang, T. Cheng, *Mater. Today Phys.* **2022**, *25*, 100701.
[40] A. Baburaj, S. K. N. Kumar, A. Kumar, M. Banakar, S. Bairagi, G. Stylios, *Nano Energy* **2023**, *118*, 108983.
[41] V. Nguyen, R. Yang, *Nano Energy* **2013**, *2*, 604.
[42] F. Shen, D. Zhang, Q. Zhang, Z. Li, H. Guo, Y. Gong, Y. Peng, *Nano Energy* **2022**, *99*, 107431.
[43] X. Zhang, M. Yu, Z. Ma, H. Ouyang, Y. Zou, S. L. Zhang, H. Niu, X. Pan, M. Xu, Z. Li, Z. L. Wang, *Adv. Funct. Mater.* **2019**, *29*, 1.
[44] S. Wang, Y. Wang, D. Liu, Z. Zhang, W. Li, C. Liu, T. Du, X. Xiao, L. Song, H. Pang, M. Xu, *Sensors Actuators, A Phys* **2021**, *317*, 112459.
[45] X. L. Zhang, Y. Dong, X. Xu, H. L. Qin, D. A. Wang, *Sci. China Technol. Sci.* **2022**, *65*, 282.
[46] W. Liu, H. Li, Q. Gao, D. Zhao, Y. Yu, Q. Xiang, X. Cheng, Z. L. Wang, W. Long, T. Cheng, *Adv. Mater.* **2023**, *35*, https://doi.org/10.1002/adma.202307184.
[47] Y. Xie, S. Wang, S. Niu, L. Lin, Q. Jing, J. Yang, Z. Wu, Z. L. Wang, *Adv. Mater.* **2014**, *26*, 6599.